Detection of pulses in a colored noise setting

Gregor Wenning, Thomas Hoch, and Klaus Obermayer
Department of Electrical Engineering and Computer Science, Technical University of Berlin, Franklinstrasse 28/29, 10587 Berlin, Germany
(Received 23 June 2004; published 8 February 2005)

Cortical neurons are exposed to a considerable amount of synaptic background activity, which increases the neurons' conductance and which leads to a fluctuating membrane potential. Here we investigate how the presence and the properties of this background noise influence the ability of a neuron to detect transient inputs, a task that is important for coincidence detection as well as for the detection of synchronous spiking events in a neural system. Using a leaky integrate-and-fire neuron as well as a biologically more realistic Hodgkin-Huxley type point neuron we find that noise enhances the detection of subthreshold input pulses and that the phenomenon of stochastic resonance occurs. When the noise is colored, pulse detection becomes more robust, because the number of false positive events decreases with increasing temporal correlation while the number of correctly detected events is almost unaffected. Therefore, the optimal variance of the noise also changes with the degree of temporal correlations of the background activity. For the integrate-and-fire model these effects can be described using an ansatz by Brunel and Sergi [J. Theor. Biol. **195**, 87 (1998)]. Numerical simulations show that the leaky integrate-and-fire model and the Hodgkin-Huxley type point neuron behave qualitatively similarly.

DOI: 10.1103/PhysRevE.71.021902 PACS number(s): 87.19.La, 05.40.−a

I. INTRODUCTION

Recent experiments and modeling studies have shown that cortical neurons receive a large number of simultaneously active inputs that give rise to so-called high conductance states and that induce strong fluctuations of the neurons' membrane potential [1]. Much work in theoretical neuroscience has been devoted to explaining this high level of background noise and to understanding its role for neural information transmission and neural computation. In previous studies it has been suggested that noise may facilitate fast information transfer through a population of neurons [2], may tune the gain of a neuron's transfer function [3], or may allow the transmission of otherwise subthreshold inputs, for example, through the phenomenon of stochastic resonance [4–16] (see [17] for a general review on stochastic resonance).

In this contribution we concentrate on the last effect of background noise and ask the question of how these background inputs contribute to the transmission and the processing of subthreshold inputs. Stochastic resonance has been experimentally observed in neural systems (see, e.g., [5,6]), and there is a lively discussion in the literature of whether this effect is actually of functional importance [7,8]. In theoretical work stationary [11], sinusoidal [4], or general continuous time-dependent inputs [18] have been considered, ways of adaptively optimizing the level of noise have been suggested [12], and stochastic resonance has been analyzed for single neurons and neuronal populations [9,13]. In most of the cases, however, the investigations dealt with the problem of information transmission rather than with the more general and maybe more adequate problem of information processing.

A simple computation a neuron can perform is the detection of pulses as they may, for example, occur through coincidences of spikes or of events of synchronous neural activity. These computations can be formulated as a special case of the task to reliably detect and respond to a transient input and have experienced increasing attention in the recent past (see, e.g., [19–21]). In particular neural synchrony [22,23] is widely believed to be an important element of cortical processing, but recent experimental findings also point to the importance of specific spike sequences [24], which may give rise to transient events if proper delays are present. But how can transient inputs be optimally detected, if a neuron is embedded in a background of noise, and how can subthreshold input pulses be transmitted using, for example, the mechanism of stochastic resonance?

Motivated by these questions, we have investigated the response of a single model neuron to brief subthreshold input pulses. Since the basic neural task is to detect a pulse we quantify the performance in terms of the detection error given by the sum of the probability of missing a pulse and the normalized number of false positive events.

This is different from the classic stochastic resonance scenario where performance is usually quantified using signal-to-noise ratios [11,25], cross-correlation measures [26], or the mutual information between input and output [18]. These approaches, however, were predominantly concerned with the reliable transmission of signals rather than with a detection task as an example of a (though still very simple) computation.

In order to make contact with the current theoretical literature, we concentrate on two approaches. First we consider a leaky integrate-and-fire (LIF) neuron, because it is simple enough to be analyzed mathematically [27,28]. Then we investigate a Hodgkin-Huxley (HH) type point neuron, because in this way we can incorporate additional effects resulting from input-driven changes in the membrane conductance [29]. In both cases, the neuron additionally receives background noise inputs, which are generated by an Ornstein-Uhlenbeck process, and which affect the membrane

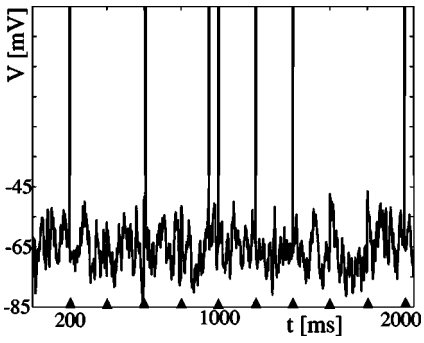

FIG. 1. Typical trace of the membrane potential of a LIF neuron, Eq. (2), which receives colored noise input [τ_X=1 ms, D =22 mV^2/ms; cf. Eq. (3)] and a train of subthreshold input pulses (5 Hz; pulse parameters, width dt=0.1 ms, height V_p=18 mV). The time of occurrence is indicated by arrowheads on the x axis for the input pulses and by vertical lines going upward for the output spikes. Threshold and reset potentials are −45 and −65 mV.

potential for the LIF (current noise) and for the HH (conductance noise) neuron models. Experimental findings [1,30] demonstrate that colored noise, rather than white noise, provides the best model for the background input. Here we also investigate the role of those temporal correlations, because only little work has been devoted to understanding the impact of these temporal correlations on neural information transmission and processing [31–34].

Our paper is organized as follows. In Sec. II we present the pulse detection scenario and we quantify pulse detection performance. The noisy LIF and HH neuron models are described in Secs. III and IV. Results for the LIF neuron are shown in Secs. V (numerical results) and VI (analytical results). The corresponding numerical results for the HH neuron are shown in Sec. VII.

II. THE PULSE DETECTION SCENARIO

We consider a single neuron, which receives a train of subthreshold pulses and additive colored noise as inputs. The details of the neuron models are described in the following sections; here we consider the problem of pulse detection.

The input pulse train is regular, but the time interval between two successive pulses is large compared to the membrane time constant and to the time constant of the temporal correlation of the additive noise, so that the preceding pulse has no significant influence on the following one. Figure 1 shows a typical trace of the resulting membrane potential for the case of the LIF model. The input pulses are marked by arrowheads on the x axis; the output spikes are marked by the vertical lines going upward and crossing the spike threshold of the neuron. The trace shows that there are several incidences where an input pulse is immediately followed by a spike. We will call this pair of events a correctly detected pulse. However, there are also several incidences where the neuron does not respond to the pulse or where a spike occurs in the absence of a signal input. If we interpret the presence of a spike as a signature for the presence of an input pulse, the latter events correspond to the errors the neuron makes in the detection task.

In order to quantify the neuron's response to the pulse train we consider the total error. The total error is the sum of a term that is proportional to the number of the false positive events and a term that is proportional to the number of pulses that are not detected, i.e., that are not immediately followed by an output spike (see the sections on the LIF and HH neurons for details). Let us consider a regular pulse train which consists of n equidistant pulses, separated by a time interval ΔT. The fraction P_m of missed pulses is then given by $P_m=1-P_c$, when P_c is the fraction of correctly detected pulses. The total number of false positives, divided by the total number of input pulses, is denoted as P_f. (Note that P_f can easily take on values larger than 1.) We then define the total error Q for pulse detection as the sum

$$Q = P_m + P_f. \tag{1}$$

Note that the value of Q depends indirectly on the interpulse interval ΔT. For longer intervals ΔT but fixed n more false positive events are likely to occur, so that the total error grows with increasing ΔT.

III. THE LIF MODEL WITH COLORED NOISE

In the LIF neuron model (see [27,29] for an introduction), the membrane potential V_t of the neuron changes in time according to the differential equation

$$\frac{dV_t}{dt} = -\frac{1}{\tau_V}(V_t - V_{reset}) + X_t, \tag{2}$$

where τ_V is the membrane time constant and X_t is the noise input at time t. Throughout this contribution we use τ_V =5 ms. Once the membrane potential reaches a threshold V_{th} (V_{th}=−45 mV), a spike is generated and the membrane potential is reset to V_{reset} (V_{reset}=−65 mV).

The noise input X_t is given by an Ornstein-Uhlenbeck process (see [27] for an introduction), which corresponds to low-pass filtered white noise with a time constant τ_X and a diffusion coefficient D,

$$\frac{dX_t}{dt} = -\frac{1}{\tau_X}X_t + \sqrt{D}\frac{dW_t}{dt}. \tag{3}$$

dW_t are the infinitesimal increments of the Wiener process. Equations (2) and (3) are solved using the Euler integration scheme (see Appendix A). Figure 2 shows a typical trace of the membrane potential for colored noise input with two different time constants τ_X.

The signal input is modeled as a series of narrow rectangular pulses with width τ_p (τ_p=0.1 ms) which generate a voltage jump of variable height V_p. These pulses are injected with a repetition frequency of $1/\Delta T$, where ΔT is the time interval between two subsequent pulses. A pulse is said to be detected if the membrane potential reaches the threshold within 0.1 ms after the injection of the current pulse. Different noise conditions are modeled by changing the time constant τ_x and the diffusion coefficient D of the Ornstein-Uhlenbeck process. If the spike process is omitted, i.e., if we only consider the unconstrained dynamics of the membrane potential, Eqs. (2) and (3), a change in the parameters τ_X and

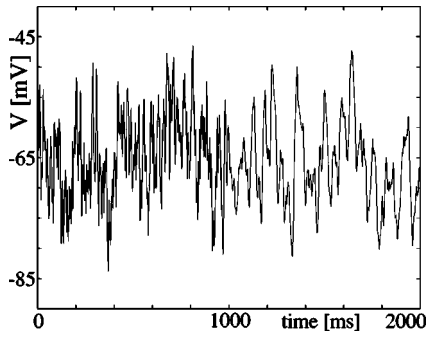

FIG. 2. Trace of the membrane potential of a LIF neuron for colored noise inputs with the two different time constants $\tau_X = 1$ ms (0–1000 ms) and $\tau_X = 10$ ms (1000–2000 ms). The diffusion coefficient D was adjusted to keep the variance of the membrane potential constant, $D = 2.2\ \mathrm{mV}^2/\mathrm{ms}$ (left) and $D = 0.04\ \mathrm{mV}^2/\mathrm{ms}$ (right).

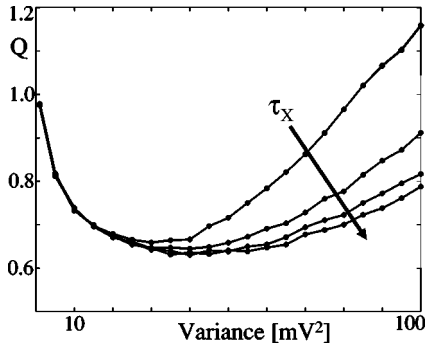

FIG. 3. Total error Q, Eq. (1), as a function of the variance of the membrane potential, Eq. (13), for the LIF model for different values of τ_X ($\tau_X = 1, 5, 10, 15$ ms). D is adjusted to keep the variance of V_t [see Eq. (13)] constant when τ_X is changed. $V_p = 18$ mV, $\Delta T = 200$ ms. Simulation results for Q were obtained by integrating Eqs. (2) and (3) and including the spike-reset process.

D affects the variance of V_t but not its mean. The relation between the variance of V_t and the parameters of the Ornstein-Uhlenbeck process is given in Eq. (13) in Sec. VI A. We will use the variance value in order to characterize the "strength" of the noise.

IV. THE HH POINT NEURON WITH COLORED NOISE

In the HH point neuron model (see [29,35] for an introduction), the membrane potential V changes in time according to the differential equation

$$C_m \frac{\partial V_t}{\partial t} = -I_L - I_{\mathrm{Na}} - I_{\mathrm{K}} - I_M - I_{syn} - I_{stim}. \tag{4}$$

The left hand side of this equation describes the influence of the membrane's capacitance C_m, while all ionic currents through the cell's membrane, including the synaptic noise (I_{syn}) and the synaptic stimulus (I_{stim}) currents, are summed on the right hand side. Following [30] we consider the following intrinsic currents: a leak current $I_L = -g_L(V - E_L)$, the spike-generating sodium (I_{Na}) and potassium (I_{K}) currents, and a noninactivating potassium current (I_M) which is responsible for spike frequency adaptation. Details of the intrinsic currents and model parameters are listed in Appendix B. They were chosen according to [30,36] and are consistent with available experimental data from neocortical pyramidal neurons.

The total synaptic noise current I_{syn} is generated by fluctuating synaptic conductances. These conductances are thought to be induced by stochastic spike trains which arrive at the excitatory and the inhibitory synapses of the neuron. Following [30] we set

$$I_{syn} = g_{et}(V_t - E_e) + g_{it}(V_t - E_i), \tag{5}$$

where g_{et} and g_{it} are the conductances of the excitatory (e) and inhibitory (i) synapses, and E_e and E_i are the corresponding reversal potentials. The time-dependent conductances are effectively described as an Ornstein-Uhlenbeck process

$$\frac{dg_{et}}{dt} = -\frac{1}{\tau_e}[g_{et} - \alpha g_{e0}] + \alpha\sqrt{D_{e0}}\frac{dW_t}{dt}, \tag{6}$$

$$\frac{dg_{it}}{dt} = -\frac{1}{\tau_i}[g_{it} - \alpha g_{i0}] + \alpha\sqrt{D_{i0}}\frac{dW_t}{dt}, \tag{7}$$

where τ_e, τ_i are the time constants, g_{e0}, g_{i0} are the average values of the synaptic conductances, and D_{e0}, D_{i0} are the diffusion coefficients. Different noise conditions are modeled by changing the synaptic conductances and the square root of the diffusion coefficient by a common gain factor α. Since the Ornstein-Uhlenbeck process models the cumulative effect of many stochastic processes this corresponds to a simplistic model of the effect of increasing the synaptic peak conductances. The parameters of the Ornstein-Uhlenbeck processes are chosen in such a way that they resemble *in vivo*–like activity [30] (see Appendix B).

The average synaptic noise current is balanced, i.e., it is zero just below threshold (3.5 mV) because the inhibitory and the excitatory currents have opposite sign but equal strength. If the mean impacts of excitation and inhibition cancel, a change in the parameter α leads to a change in the higher moments of the fluctuations of the membrane potential only. For other values of V_t, however, a change in α also induces a shift of the average value of V_t.

The signal input I_{stim} is modeled as a series of narrow rectangular current pulses with width τ_p ($\tau_p = 0.4$ ms), with variable strength I_p, and with a repetition frequency of $1/\Delta T$, where ΔT is the time interval between two pulses. A current pulse is said to be detected if the HH neuron spikes within 5 ms after the application of a current pulse.

V. LEAKY INTEGRATE-AND-FIRE MODEL: RESULTS

Figure 3 shows the total error Q as a function of the variance of the unconstrained membrane potential for different values of the time constant τ_X of the noise. In case of the LIF neuron we refer to the "variance of the membrane potential" when the variance is calculated according to Eq. (13), without the spike-reset mechanism. The diffusion coefficient D was always adjusted to keep the variance of V_t [see Eq. (13)] constant when τ_X was changed. The figure demonstrates that stochastic resonance curves emerge, and that the

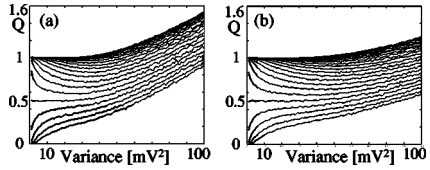

FIG. 4. Total error Q, Eq. (1), as a function of the variance of the membrane potential, Eq. (13), for the LIF model for the case of short-, $\tau_X=1$ ms, (a) and long-range, $\tau_X=10$ ms, (b), temporal correlations. Different lines correspond to different pulse heights $V_p=1,2,3,\ldots,24$ mV (top to bottom). $\Delta T=200$ ms. Pulses that induce voltage jumps smaller than 20 mV are subthreshold. Simulation results are obtained by directly integrating Eqs. (2) and (3) and including the spike-reset process.

presence of temporal correlations (finite values of τ_X) improves pulse detection. If τ_X becomes larger, the minimum of Q decreases and becomes more shallow. The latter effect makes pulse detection more robust against a suboptimal choice of the variance of V_t.

Figure 4 shows the total error Q as a function of the variance of the membrane potential for several pulse heights and for short- [Fig. 4(a)] as well as long-range [Fig. 4(b)] temporal correlations of the noise. If input pulses are strong enough to make the neuron fire, performance is best if no noise is present. For subthreshold (except for the weakest) pulses, stochastic-resonance-like curves appear and a finite optimal strength of the noise exists.

Figure 5 shows the fraction P_m of missed pulses [Fig. 5(a)], and the fraction P_f of false positives [Fig. 5(b)] as a function of the variance of the membrane potential, again for different values of the time constant τ_X. The temporal correlations of the noise inputs do not affect the number of missed detections; improved performance is exclusively due to a decrease in the number of false positives.

Figure 6 shows the optimal noise level in terms of the variance of the unconstrained membrane potential as a function of the height of the input pulses. The lower and upper curves correspond to $\tau_X=1$ and 10 ms. Pulses that induce jumps larger than 20 mV are suprathreshold, and any noise inputs are detrimental. Below $V_p=20$ mV one observes a nonmonotonic dependence of the optimal noise level on the strength of the input pulses and a pronounced maximum for intermediate pulse heights. For larger values of τ_X, the maximum shifts to larger noise levels. We will discuss these findings in more detail in Sec. VI D (e.g., Fig. 10).

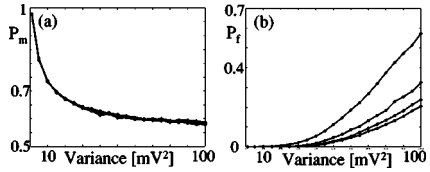

FIG. 5. Fraction P_m of missed pulses (a) and the normalized number P_f of false positives (b) as a function of the variance of the membrane potential, Eq. (13), for the LIF neuron. Different curves correspond to different choices of the parameter $\tau_X=1$, 5, 10, 15 ms. D was again adjusted to keep the variance of V_t constant. Pulse train parameters as in Fig. 3. Simulation results are obtained by directly integrating Eqs. (2) and (3) and including the spike-reset process.

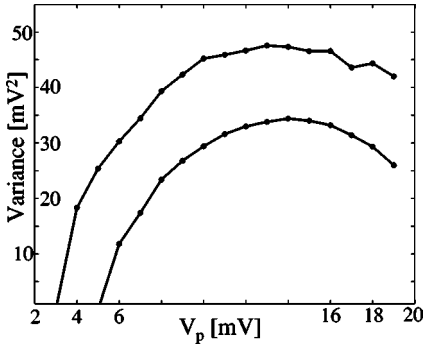

FIG. 6. Optimal noise level for signal detection, in terms of the total error Q, as a function of the height of the input pulses for the LIF model. The upper and lower curves correspond to $\tau_X=10$ and 1 ms. For small pulse heights and for pulse heights $\geqslant 20$ mV the optimal noise level is zero. Simulation results are obtained by directly integrating Eqs. (2) and (3) and including the spike-reset process.

VI. ANALYSIS OF THE LIF MODEL

A. Second-order moments

In order to derive expressions for the second moments $\langle X_t^2\rangle$, $\langle X_t V_t\rangle$, and $\langle V_t^2\rangle$ ($\langle\ \rangle$ denotes an ensemble average) we consider the discrete version (Euler integration) of Eqs. (2) and (3),

$$X_{t+1} = X_t - \frac{1}{\tau_X} X_t dt + \sqrt{D} dW_t, \tag{8}$$

$$V_{t+1} = V_t - \frac{1}{\tau_V} V_t dt + X_t dt, \tag{9}$$

in the absence of the fire-and-reset mechanism, where dW_t are the infinitesimal increments of the Wiener process. After multiplication of the left and right hand sides of Eqs. (8) and (9) and after taking an ensemble average we obtain

$$\frac{d\langle X_t^2\rangle}{dt} + \frac{2}{\tau_X}\langle X_t^2\rangle = D, \tag{10}$$

$$\frac{d\langle X_t V_t\rangle}{dt} + \frac{1}{\tilde{\tau}}\langle X_t V_t\rangle = \langle X_t^2\rangle, \quad \tilde{\tau} = \frac{\tau_X \tau_V}{\tau_X + \tau_V}, \tag{11}$$

$$\frac{d\langle V_t^2\rangle}{dt} + \frac{2}{\tau_V}\langle V_t^2\rangle = 2\langle X_t V_t\rangle, \tag{12}$$

where we made use of the fact that $\langle X_t dW_t\rangle = 0$ and where all terms of order larger than 1 in dt were neglected [37]. The stationary state is then given by

$$\langle X_t^2\rangle = \frac{D\tau_X}{2}, \quad \langle X_t V_t\rangle = \frac{D\tau_X\tilde{\tau}}{2}, \quad \langle V_t^2\rangle = \frac{D\tau_X\tau_V\tilde{\tau}}{2}. \tag{13}$$

B. Probability of correct detection

Equations (13) describe the second moment of the membrane potential in the absence of pulses and the firing-and-

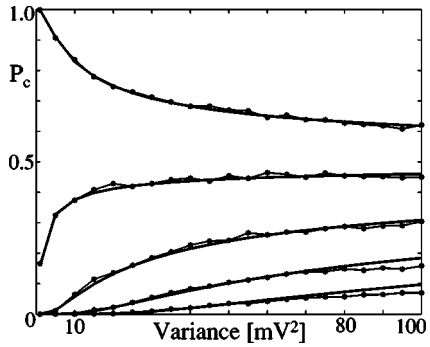

FIG. 7. Fraction of correctly detected input pulses as a function of the variance of the membrane potential for the LIF model. Thin solid line with dots: fraction of correctly detected input pulses by numerical evaluation of Eqs. (2) and (3) including the spike-reset process. Thick solid line: probability of correct detection according to Eq. (14). The variance σ_V^2 of the membrane potential was changed by changing D. The different pairs of lines correspond to $V_p = 7$, 11, 15, 19, 23 mV. Pulses that induce changes that are larger than 20 mV are suprathreshold. $\Delta T = 200$ ms, $\tau_X = 1$ ms.

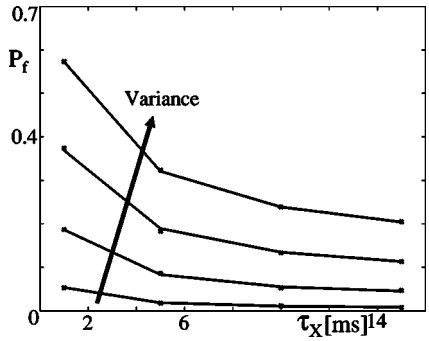

FIG. 8. Normalized number P_f of false positives versus τ_X. The vertices of the solid polygon show P_f [according to Eq. (15)] for different values of the membrane potential variances $\sigma_V^2 = 40, 60, 80, 100$ mV^2 (bottom to top). Crosses: numerical evaluation of Eqs. (2) and (3) including the spike-reset process. For one line, D was always adjusted to keep the variance σ_V^2 constant.

reset mechanism. We now describe the stationary probability distribution of the fluctuating membrane potential by a Gaussian distribution with its mean set to the reset potential −65 mV and with variance $\sigma_V^2 = \frac{1}{2} D \tau_X \tau_V \tilde{\tau}$. If a narrow input pulse arrives, the membrane potential is instantaneously shifted by an amount V_p, and the probability that the membrane potential becomes suprathreshold is given by

$$P_c = 0.5 \operatorname{erfc}\left(\frac{V_{th} - V_p - V_{reset}}{\sqrt{2}\sigma_V} \right), \tag{14}$$

which is equal to the probability of correct detection; erfc is the complementary error function.

Figure 7 shows the fraction P_C of correctly detected pulses according to a numerical evaluation of Eqs. (2) and (3) in comparison with the probability of correct detection calculated according to Eq. (14). Equation (14) provides a good approximation of P_C for sub- as well as for suprathreshold input pulses. Small deviations from Eq. (14) occur for large values of $\langle V_t^2 \rangle$ and small pulse heights. In this regime the Gaussian assumption for the membrane potential distribution is violated.

C. False positive rate

If V_p is set to 0 mV, Eq. (14) corresponds to the probability of emitting a false positive spike. If this probability is high, however, the above approach is no longer appropriate because it discards the effects of a prolonged probability flux across the threshold. A better result can be obtained using an approach suggested by Brunel and Sergi [28].

Brunel and Sergi provide expressions for the spiking frequency of a LIF neuron with low-pass filtered Gaussian white noise, as described by Eqs. (2) and (3). They show that the spike frequency of such a neuron can be reduced to that of a basic LIF neuron ($\tau_X = 0$) using an *effective* threshold θ_{eff}. For values of $\tau_X > 0$ the effective threshold is given by the sum of the threshold θ and two correction terms of first and second order in $\sqrt{\tau_X / \tau_V}$, as demonstrated in their paper.

Using $\psi(w) = \exp(w^2)[\operatorname{erf}(w) + 1]$ and $\sigma = \sqrt{D \tau_V \tau_X}$ the mean first passage time $\langle T_f \rangle$ according to [28] is

$$\langle T_f \rangle = \tau_V \sqrt{\pi} \int_{V_{reset}/\sigma}^{\theta_{eff}/\sigma} \psi(w) dw, \tag{15}$$

in which θ_{eff},

$$\theta_{eff} = \theta + \sigma(\nu_1 k + \nu_2 k^2), \quad k = \sqrt{\frac{\tau_X}{\tau_V}}, \tag{16}$$

is the effective threshold with parameters ν_1 and ν_2, which are determined using a least-squares fitting procedure (see Appendix C).

P_f is then given by the expected number of spikes in an interpulse interval, $P_f = \Delta T / \langle T_f \rangle$.

Figure 8 shows P_f as a function of τ_X for different values of the [unconstrained, Eq. (13)] membrane potential. The number of false positive events decreases with increasing τ_X and the effect is nicely predicted by Eqs. (15) and (16). This reduction is caused by a reduction of the number of rapid and large fluctuations of the membrane potential. After a reset to V_{reset} it takes more time on average for the membrane potential to reach the threshold again [cf. Eq. (15)].

D. Quality of pulse detection

Figure 9 shows the number P_f of false positive events per input pulse, and the total error Q as a function of the variance, Eq. (13), of the membrane potential and for different values of the correlation time constant τ_X. Results obtained by integration of Eqs. (2) and (3) including the spike-reset mechanism and results obtained by evaluating Eqs. (14) and (15) are superimposed. The number of false positive events per input pulse decreases with increasing time constant of the temporal correlation [see Fig. 9(a)]. The total error Q is plotted in Fig. 9(b). It shows a minimal value at an optimal value of σ_V, which—however—depends on τ_X. When τ_X increases, the number of false positives becomes smaller and the total

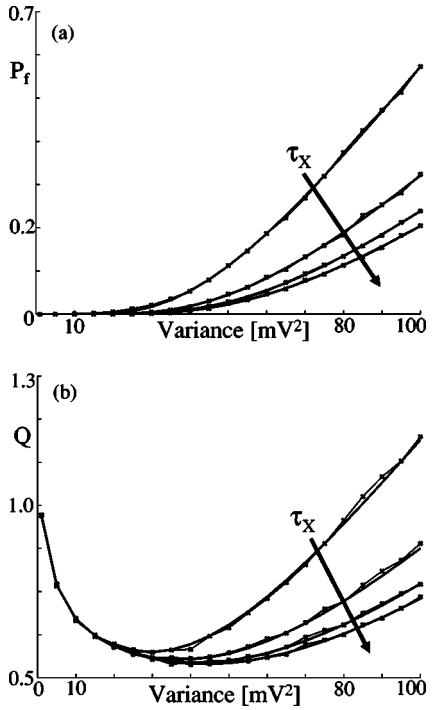

FIG. 9. Number of false positive events per input pulse (a) and the total error Q (b) as a function of the variance σ_V^2 of the membrane potential for the LIF model. Thick (and smooth) lines denote the results obtained with Eqs. (14) and (15), thin (and wiggly) lines with small crosses denote the results obtained by integrating Eqs. (2) and (3), including the spike and reset process. Different pairs of lines, from top to bottom in (a) and (b), correspond to τ_X=1, 5, 10, 15 ms. The values of ν_1 and ν_2 are given in Appendix C. Parameters are V_p=18 mV, ΔT=200 ms, other parameters as in Fig. 5.

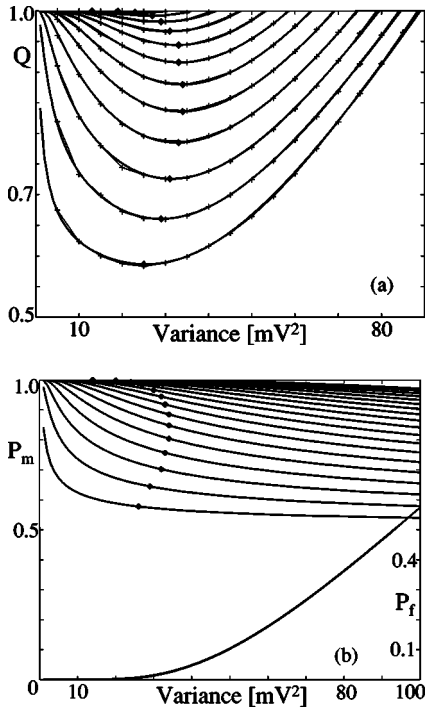

FIG. 10. Total error Q, the normalized number P_f of false positive events, and the probability P_m of not detecting an input pulse, as a function of the variance σ_V^2 of the unconstrained membrane potential. Different curves correspond to pulse heights V_p =6,7,…,19 mV (top to bottom). Dots indicate the optimal value of σ_V^2, i.e., the minimum of the total error Q. (a) Thin (and wiggly) lines with small crosses: simulation results for Q obtained by directly integrating Eqs. (2) and (3) and including the spike-reset process. Thick (and smooth) lines: results for Q are obtained by evaluating Eqs. (14) and (15). (b) P_m (top curves) and P_f (bottom curves) calculated according to Eqs. (14) and (15). Parameters are τ_X=1 ms, ΔT=200 ms.

error decreases, too. The parameters ν_1 and ν_2 from Eq. (15) were fitted using the least-squares method (parameters and details are given in Appendix C).

In Fig. 6 we have shown that the optimal noise level, i.e., the optimal value for σ_V, is a nonmonotonic function of the pulse height V_p. This effect is also well described by Eqs. (14) and (15). Figure 10 shows the total error Q, the normalized number P_f of false positive events, and the probability P_m of not detecting an input pulse, as a function of the variance σ_V^2 of the membrane potential and for different values of the height V_p of the input pulses. The optimal level for the variance of the membrane potential is indicated by dots. Since P_f does not depend on the signal input, the nonmonotonic dependence of the optimal variance is due to changes in P_m only. A characteristic of the optimal noise level is that the slopes of P_f and P_m versus the membrane potential variance match each other. P_f as a function of the noise level first starts with a very small slope, but grows vigorously with increasing noise. In the regime where P_f starts growing, P_m has a small slope for very weak pulses and large subthreshold pulses. For intermediate pulse heights, the slope of P_m versus the membrane potential variance is larger; thus the optimal noise level is shifted to higher values.

VII. SIMULATION RESULTS FOR THE HODGKIN-HUXLEY MODEL

In this section we investigate, whether and under what conditions the predictions of the LIF model carry over to the biophysically more realistic HH framework. The correlation structure of the noise inputs for the HH model is more complicated than for the LIF model. It must be described by two time constants, one for the excitatory, τ_e, and one for the inhibitory, τ_i, synaptic inputs [Eqs. (6) and (7)]. As a consequence of this and of the fact that the HH model is mathematically more complicated, no exact closed expression can be derived for the variance of the membrane potential as a function of the other model parameters. We, therefore, adopted the following strategy. We chose a value for α, Eqs. (6) and (7), which is small enough (α=0.3) so that the membrane potential remains subthreshold. We then constructed—by trial and error—three sets $\{\tau_e, \tau_i, D_{e0}, D_{i0}\}$ of parameters (see caption of Fig. 11). First the correlation structure of the noise inputs was changed by changing the values of the excitatory and inhibitory time constants. Then the diffusion constants were adjusted so that the variances of

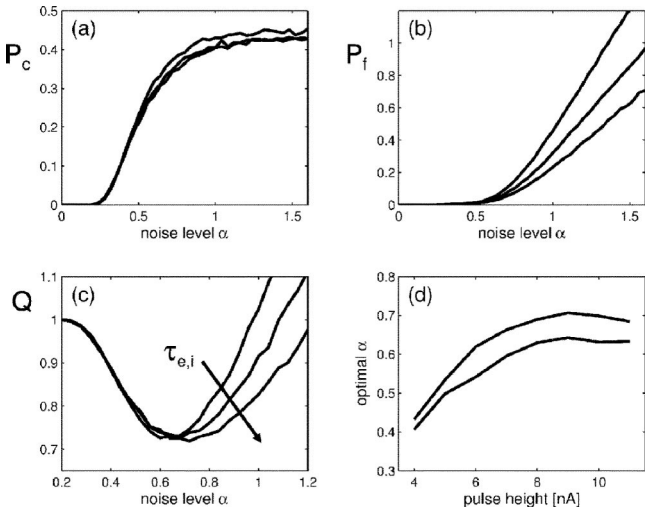

FIG. 11. Characterization of the pulse detection performance of the HH model neuron. The fraction P_c of correctly detected events (a), the normalized number P_f of false positive events (b), and the total error Q (c) is plotted as a function of the noise parameter α. (a)–(c) The three different curves in each figure correspond to three sets of parameters; see the text for details. Parameters were $(\tau_{e0},\tau_{i0})=\beta(2.7,10.5)$ms, $(D_{e0},D_{i0})=\gamma(41.7,51.9)$ nS^2/ms, with $(\beta,\gamma)=(0.5,1.32)$, (1,1), (2,0.82). Pulse height $I_p=10$ nA, interpulse interval $\Delta T=200$ ms. (d) Optimal value of α for pulse heights $I_p=4-11$ nA, and $(\beta,\gamma)=(0.5,1.32)$ (bottom curve) and (2, 0.82) (top curve). Other parameters as for (a)–(c). Pulses are suprathreshold for $I_p>11$ nA. $(\tau_{e0},\tau_{i0})=(2.7,10.5)$ ms was taken from [30] as an estimate for a layer VI pyramidal cell in the cat parietal cortex.

the membrane potential—determined by numerically integrating Eq. (4)—matched each other. Pulse detection performance was then evaluated as a function of the parameter α with all the other parameters being constant [cf. Eqs. (6) and (7)]. When α is increased, the variance of the membrane potential becomes larger while the average value of V remains (approximately) constant. When α becomes really large, however, spiking activity strongly contributes to the temporal changes of the membrane potential, and its variance is no longer a proper measure. α on the other hand still is a good parameter for measuring the strength of noise.

Figure 11 shows the results. In Figs. 11(a) and 11(b) the fraction P_c of correct detections and the normalized number P_f of false positive events are plotted as a function of the noise parameter α and for the three sets of parameters described above. The results are qualitatively similar to the results of the LIF model. The fraction of correctly detected events increases with increasing strength of the conductance noise, and the dependency is almost unaffected by the properties of the temporal correlations. With higher noise, the normalized number of false positive events increases, but stronger temporal correlations lead to a reduction similar to what is observed for the LIF neuron. Figure 11(c) shows the corresponding "stochastic resonance" curves for the total error Q. The optimal noise level changes with the height I_p of the input pulses in a nonmonotonic fashion [Fig. 11(d)], similar to the results for the LIF case.

VIII. CONCLUSION

In this contribution we have demonstrated that the structure of the temporal correlations (the "color") of the membrane potential has a significant impact on pulse detection performance. Using a sum of missed pulses and false positive events we showed that a leaky integrate-and-fire neuron as well as a biophysically more realistic Hodgkin-Huxley type neuron behave in a similar way. Increasing the correlation time constants of the additive noise makes the detection of subthreshold pulses more robust. The number of false positive events is reduced and the optimal value of the noise parameter (variance of the membrane potential for the LIF and the noise parameter α for the HH model) is shifted to higher values. The optimal noise level is not a monotonic function of the strength of the input signal.

The total error, which is the sum of the fraction of "missed" pulses (false negatives) and the number of false positive events per interpulse interval, is always larger than 0.5. This is a consequence of the zero mean noise. The probability that an otherwise subthreshold input pulse gets enhanced by a positive fluctuation is equal to the probability that it is further suppressed by its negative counterpart. Therefore, the probability of correct detection can never exceed 0.5. Because of this fact one can question the biological relevance of the described pulse detection scenario for single neurons. In the case of populations of neurons, however, weak transient excitations can be reliably detected and corresponding results will be reported in a subsequent study.

ACKNOWLEDGMENTS

We thank Jacob Kanev for inspiring discussions. This work was supported by DFG (SFB 618).

APPENDIX A: EULER APPROXIMATION OF THE WIENER PROCESS

$dW_t=N_t\sqrt{dt}$, where N_t is a normal random variable, variance 1, and dt corresponds to the length of the time interval in a standard Euler scheme. For the exact numerical integration of an Ornstein-Uhlenbeck process see [37].

APPENDIX B: THE HODGKIN-HUXLEY NEURON

$$C_m\frac{\partial V}{\partial t}=-I_L-I_{\mathrm{Na}}-I_{\mathrm{K}}-I_M-I_{syn}+I_{stim,t}, \qquad \text{(B1)}$$

where the leak current $I_L=g_L(V-E_L)$, and the model parameters are $C_m=1\ \mu\mathrm{F/cm}^2$, $g_L=0.045$ mS, and $E_L=-80$ mV.

Voltage-dependent sodium current I_{Na}

$$I_{\mathrm{Na}}=\bar{g}_{\mathrm{Na}}m^3h(V-E_{\mathrm{Na}}),$$

$$\frac{dm}{dt}=\alpha_m(V)(1-m)-\beta_m(V)m,$$

$$\frac{dh}{dt} = \alpha_h(V)(1-h) - \beta_h(V)h,$$

$$\alpha_m(V) = \frac{-0.32(V - V_T - 13)}{\exp[-(V - V_T - 13)/4] - 1},$$

$$\beta_m(V) = \frac{0.28(V - V_T - 40)}{\exp[-(V - V_T - 40)/5] - 1},$$

$$\alpha_h(V) = 0.128 \exp[-(V - V_T - V_S - 17)/18],$$

$$\beta_h(V) = \frac{4}{1 + \exp[-(V - V_T - V_S - 40)/5]}.$$

Model parameters are $\bar{g}_{\mathrm{Na}}=3$ mS/cm^2, $V_T=-58$ mV and $V_S=-10$ mV, $E_{\mathrm{Na}}=0$ mV.

Delayed-rectifier potassium current I_{K}

$$I_{\mathrm{K}} = \bar{g}_{\mathrm{K}} n^4 (V - E_{\mathrm{K}}),$$

$$\frac{dn}{dt} = \alpha_n(V)(1-n) - \beta_n(V)n,$$

$$\alpha_n(V) = \frac{-0.032(V - V_T - 15)}{\exp[-(V - V_T - 15)/5] - 1},$$

$$\beta_n(V) = 0.5 \exp[-(V - V_T - 10)/40].$$

Model parameters are $\bar{g}_{\mathrm{K}}=5$ mS/cm^2 and $V_T=-58$ mV, $E_{\mathrm{K}}=-80$ mV.

Noninactivating potassium current I_M

$$I_M = \bar{g}_M p (V - E_{\mathrm{K}}),$$

$$\frac{dp}{dt} = \alpha_p(V)(1-p) - \beta_p(V)p,$$

$$\alpha_p(V) = \frac{0.0001(V + 30)}{1 - \exp[-(V + 30)/9]},$$

$$\beta_p(V) = \frac{-0.0001(V + 30)}{1 - \exp[(V + 30)/9]}.$$

Model parameter is $\bar{g}_M=1$ μS/cm^2.

Synaptic noise current

$$I_{syn} = g_{et}(V - E_e) + g_{it}(V - E_i). \tag{B2}$$

Model parameters are $E_e=0$ mV, $E_i=-80$ mV.

Synaptic conductances

$$\frac{dg_{et}}{dt} = -\frac{1}{\tau_e}[g_{et} - \alpha g_{e0}] + \alpha\sqrt{D_e}\frac{dW_t}{dt}, \tag{B3}$$

$$\frac{dg_{it}}{dt} = -\frac{1}{\tau_i}[g_{it} - \alpha g_{i0}] + \alpha\sqrt{D_i}\frac{dW_t}{dt}. \tag{B4}$$

Model parameters (if not metioned otherwise) are $g_{e0}=0.0121$ μS, $g_{i0}=0.0484$ μS, $\sigma_{e0}=0.0075$ μS, $\sigma_{i0}=0.0165$ μS, $\tau_e=2.7$ ms, and $\tau_i=10.5$ ms. For the stationary membrane potential distributions the relation $\sigma^2_{e,i}=0.5(D_{e,i}\tau_{e,i})$ holds. All simulations were performed in the NEURON simulation environment [38] using the point-conductance model from Destexhe *et al.* as described in [30,36].

APPENDIX C: PARAMETERS OF THE ANSATZ BY BRUNEL AND SERGI

The values for ν_1 and ν_2, Eq. (16), were determined by a least-squares fit using the MATLAB function NLINFIT. As in [28] the values of ν_2 are a function of $\hat{\theta}=V_r/\sqrt{D_{\tau_V\tau_X}}$, i.e., $\nu_2=\nu_{2a}+\nu_{2b}\hat{\theta}$.

	$\tau_X=1$ ms	$\tau_X=5$ ms	$\tau_X=10$ ms	$\tau_X=15$ ms
ν_1	1.40	1.12	1.07	1.06
ν_{2a}	−0.19	−0.26	−0.30	−0.31
ν_{2b}	0.04	0.21	0.26	0.26

The error in the parameters due to the least-squares fit is ±0.01 (95% confidence interval).

[1] A. Destexhe, M. Rudolph, and D. Paré, Nat. Rev. Neurosci. **4**, 1 (2003).
[2] M. Tsodyks and T. Sejnowski, Network Comput. Neural Syst. **6**, 111 (1995).
[3] F. Chance and A. Reyes, Neuron **35**, 773 (2002).
[4] A. Longtin, J. Stat. Phys. **70**, 309 (1993).
[5] D. F. Russel, L. A. Wilkens, and F. Moss, Nature (London) **402**, 291 (1999).
[6] J. K. Douglass, L. Wilkens, E. Pantazelou, and F. Moss, Nature (London) **365**, 337 (1993).
[7] Y. Gong, N. Matthews, and N. Qian, Phys. Rev. E **65**, 031904 (2002).
[8] J. Tougaard, Biol. Cybern. **83**, 471 (2000).
[9] J. J. Collins, C. C. Chow, and T. T. Imhoff, Nature (London) **376**, 236 (1995).
[10] T. Mori and S. Kai, Phys. Rev. Lett. **88**, 218101 (2002).
[11] M. Stemmler, Network Comput. Neural Syst. **7**, 687 (1996).
[12] G. Wenning and K. Obermayer, Phys. Rev. Lett. **90**, 120602 (2003).
[13] T. Hoch, G. Wenning, and K. Obermayer, Phys. Rev. E **68**, 011911 (2003).
[14] Adi R. Bulsara, Tim C. Elston, Charles R. Doering, Steve B.

Lowen, and Katja Lindenberg, Phys. Rev. E **53**, 3958 (1996).
[15] H. E. Plesser and T. Geisel, Phys. Rev. E **59**, 7008 (1999).
[16] B. Lindner and L. Schimansky-Geier, Phys. Rev. Lett. **86**, 2934 (2001).
[17] L. Gammaitoni, P. Hänggi, P. Jung, and F. Marchesoni, Rev. Mod. Phys. **70**, 223 (1998).
[18] A. R. Bulsara, and A. Zador, Phys. Rev. E **54**, R2185 (1996).
[19] M. Rudolph and A. Destexhe, J. Comput. Neurosci. **14**, 239 (2003).
[20] M. Rudolph and A. Destexhe, Phys. Rev. Lett. **86**, 3662 (2001).
[21] M. Diesmann, M. O. Gewaltig, and A. Aertsen, Nature (London) **402**, 529 (1999).
[22] M. Abeles, E. Vaadia, H. Bergman, Y. Prut, I. Haalman, and H. Slovin, Concepts Neurosci. **4**, 131 (1993).
[23] A. K. Engel, P. Fries, and W. Singer, Nat. Rev. Neurosci. **2**, 704 (2001).
[24] M. Stopfer, V. Jayaraman, and G. Laurent, Neuron **39**, 991 (2003).
[25] F. Chapeau-Blondeau, X. Godivier, and N. Chambet, Phys. Rev. E **53**, 1273 (1996).
[26] C. Heneghan *et al.*, Phys. Rev. E **54**, R2228 (1996).
[27] H. C. Tuckwell, *Introduction to Theoretical Neurobiology: Volume 2, Nonlinear and Stochastic Theories* (Cambridge University Press, Cambridge, U.K., 1998)
[28] N. Brunel and S. Sergi, J. Theor. Biol. **195**, 87 (1998).
[29] P. Dayan and L. F. Abbott, *Theoretical Neuroscience: Computational and Mathematical Modeling in Neural Systems* (MIT Press, Cambridge, MA, 2001).
[30] A. Destexhe, M. Rudolph, J.-M. Fellous. and T. J. Sejnowski, Neuroscience **107**, 13 (2001).
[31] D. Nozaki, D. J. Mar, P. Grigg, and J. J. Collins, Phys. Rev. Lett. **82**, 2402 (1999).
[32] A. Capurro, K. Pakdaman, T. Nomura, and S. Sato, Phys. Rev. E **58**, 4820 (1998).
[33] G. Mato, Phys. Rev. E **58**, 876 (1998).
[34] N. Brunel, F. S. Chance, N. Fourcaud, and L. F. Abbott, Phys. Rev. Lett. **86**, 2186 (2001).
[35] *Methods in Neural Modeling*, edited by C. Koch and I. Segev (MIT Press, Cambridge, MA, 1998).
[36] A. Destexhe and D. Pare, J. Neurophysiol. **81**, 1531 (1999).
[37] D. T. Gillespie, Phys. Rev. E **54**, 2084 (1996).
[38] M. L. Hines and N. T. Carnevale, Neural Comput. **9**, 1179 (1997); The code for the original model is available from http://senselab.med.yale.edu/senselab/